MODELING of the MEASUREMENT CONTROL PROCESS in EDDY-CURRENT STRUCTROSCOPY USING APRIORI INFORMATION ABOUT OBJECTS

Volodymyr Ya. Halchenko [1], Ruslana V. Trembovetska [1], Volodymyr V. Tychkov [1], and Natalia B. Tychkova [1]

[1] *Cherkasy State Technological University, 460 Shevchenko Blvd., Cherkasy, 18006, Ukraine*

Abstract
Based on the proposed methodology, the essence of which is to determine the profiles of electrophysical parameters of cylindrical objects of eddy-current testing by means of surrogate optimization in a compact PCA-space search of reduced dimensionality, the modeling of the measurement control process was carried out using the accumulated apriori information about the object. The peculiarity of these studies is the consideration of previously collected information on the patterns caused by profile variations. The functions of an accumulator and carrier of apriori information were performed by a metamodel based on deep MLP-neural networks, which is characterized by a high computational efficiency. Modelling on numerical experiments have proved the feasibility of the proposed approach to improving the method for determining the distributions of magnetic permeability and electrical conductivity along the near-surface layer of a metal object with changes in microstructure. The results analysis of modeling of the inverse measurement problem indicates a sufficiently high accuracy of profile reconstruction.

Keywords
Magnetic permeability and electrical conductivity profiles, eddy-current measurement control, apriori information, surrogate optimization, PCA-space, metamodel, deep neural networks.

1. Introduction

Information on the structural condition of objects, products, and materials is in demand in many industries. Knowledge of the structural features makes it possible to timely diagnose objects and make conclusions about their trouble-free operation period, control the quality of various technological processes, including, for example, strengthening of the objects surface, identifying places of uncontrolled temperature impact on objects, etc. A non-destructive method of obtaining such information is important. It is known that microstructural changes in metals are closely related to their electrophysical parameters, which can be measured by the eddy-current method [1, 2]. The information content of the structure can be more complete if the measurements result in the distribution of electrical conductivity (EC) and magnetic permeability (MP) along the thickness of the material, i.e., EC and MP profiles. Testing objects (TO) of cylindrical shape in industry account for a significant proportion. Therefore, a simultaneous determination of the profiles of electrophysical parameters along their radius at a certain thickness of their near-surface layer is an applied problem relevant for industry.

Scientists pay primary attention to this problem, but it remains not fully studied. The authors analyzed the state of research conducted in this area quite thoroughly in [3, 4], where their main trends were identified. Some modern approaches to solving the problem are largely focused on the use of

physical measurements by eddy-current probes (ECP) at several [5, 6] or time-varying [7, 8] excitation frequencies. This introduces additional difficulties in the quite complex signal processing algorithms and complicates the hardware of the measuring systems. All these disadvantages can be eliminated by applying the measurement method with the accumulation of a priori information on the TO, which is given in the article [3] of the authors. Articles [3, 9, 10] describe the implementation of this method in detail, but at the last stage of determining the profiles, the LUT (Lookup Table) method [11] was used to solve the problem in real time, which is known to have certain limitations on the accuracy of finding a solution.

In these studies, the problem is solved by means of an optimization method, which consists in minimizing a quadratic function that, by varying the parameters of the desired profiles, leads to the actual coincidence of the results of the full-scale measurement of the ECP EMF and the one obtained by surrogate modeling [12]. Moreover, the optimization is not performed in the full space of factors, but in the PCA-space of reduced dimensionality.

Therefore, **the aim of this paper** is to study the effectiveness of the proposed surrogate optimization method as a result of computer simulation of the eddy-current measurement process of both profiles of electrophysical parameters of cylindrical testing objects using the accumulated apriori information about them obtained by preliminary modeling and stored in the metamodel.

2. The research methodology

The research methodology was discussed in detail by the authors and illustrated with examples in articles [3, 9, 10]. Let us briefly recall its main stages:

- "exact" solution of the direct electrodynamic problem of interaction of a quasi-stationary electromagnetic field generated by a passing ECP with a ferromagnetic cylindrical TO characterized by continuous profiles of electrophysical properties along the radius;

- designing of a computational experiment and construction of an apriori substitute model (metamodel) using an electrodynamic model based on deep MLP-neural networks, which is much less resource-intensive and approximates the "exact" model with acceptable accuracy;

- solving the inverse measurement problem by the optimization hybrid population metaheuristic method based on the measurements using the ECP and the surrogate model created in the previous step.

In these studies, the last stage is characterized by certain features. Surrogate optimization is not carried out in the full design space defined by the number of parameters of the desired EC and MP profiles, but in its reduced dimensional analog, which retains almost all the properties of the original one with insignificant information. This compact representation of the search space is made possible by the use of the PCA (Principal Component Analysis) method [13], which determines the main directions in the original high-dimensional space characterizing the greatest impact on data variability by linear transformations. Thus, the optimization achieves a controlled choice of the dimension of the search space, which helps find a compromise between the accuracy of the solution and its computational resource intensity.

In this case, the metamodel is created in a reduced PCA-space, which also has its advantages. At the same time, the surrogate model becomes less cumbersome, and it requires a smaller training sample to achieve sufficient accuracy of the electrodynamic model approximation. The optimization algorithm operates under the conditions of the desired variables, which are presented in a normalized form. It also adds certain improved capabilities for finding a solution to the problem.

The optimization uses a hybrid particle swarm global stochastic optimization algorithm. Therefore, the final solution of the problem is obtained by averaging their variants found by the multistart technique.

3. Electrodynamic model of the problem

The general view of the electrodynamic model in the cylindrical coordinate system, known as the Dodd-Deeds model [14], is given below and described in more detail in [3] as the Uzal-Cheng-Dodd-Deeds model, taking into account the piecewise constant representation of generally continuous profiles and their approximations by typical distributions characteristic of most practical cases:

$$E = j\omega \oint_{l_{s-coil}} \vec{A}\, dl = j\omega 2\pi r_s A(r_s, z_s),$$

where

$$A(r_s, z_s) = \frac{IN_d \mu_0 r_d}{\pi} \int_0^\infty \frac{Q1\, Q2}{\alpha^3 (U_{22} V_{11} - U_{12} V_{21})} Q3\, d\alpha,$$

$$Q1 = \sin\left(\alpha(z - l_{d1})\right) - \sin\left(\alpha(z - l_{d2})\right),$$

$$Q2 = V_{11} I_1(\alpha_n r) + V_{21} K_1(\alpha_n r),$$

$$Q3 = U_{12} I(r_{d2}, r_{d1}) + U_{22} K(r_{d2}, r_{d1}),$$

$$I(r_{d2}, r_{d1}) = \int_{\alpha r_{d1}}^{\alpha r_{d2}} t I_1(\alpha t)\, dt,$$

$$K(r_{d2}, r_{d1}) = \int_{\alpha r_{d1}}^{\alpha r_{d2}} t K_1(\alpha t)\, dt,$$

$$N_d = \frac{W}{(r_{d2} - r_{d1})(l_{d2} - l_{d1})},$$

$$V_{11}(n+1, n) = \left(K_0(\alpha_{n+1} r_n) I_1(\alpha_n r_n) + \frac{\beta_n}{\beta_{n+1}} I_0(\alpha_n r_n) K_1(\alpha_{n+1} r_n) \right) \alpha_{n+1} r_n,$$

$$V_{21}(n+1, n) = \left(I_0(\alpha_{n+1} r_n) I_1(\alpha_n r_n) - \frac{\beta_n}{\beta_{n+1}} I_0(\alpha_n r_n) I_1(\alpha_{n+1} r_n) \right) \alpha_{n+1} r_n,$$

$$U_{12}(n+1, n) = \left(K_0(\alpha_{n+1} r_n) K_1(\alpha_n r_n) - \frac{\beta_n}{\beta_{n+1}} K_0(\alpha_n r_n) K_1(\alpha_{n+1} r_n) \right) \alpha_{n+1} r_n,$$

$$U_{22}(n+1, n) = \left(I_0(\alpha_{n+1} r_n) K_1(\alpha_n r_n) + \frac{\beta_n}{\beta_{n+1}} K_0(\alpha_n r_n) I_1(\alpha_{n+1} r_n) \right) \alpha_{n+1} r_n,$$

$$\beta_n = \left(\frac{\mu_0}{\mu_n} \right) \alpha_n,$$

$$\alpha_n = \sqrt{\alpha^2 - j\mu_n \sigma_n}, \quad n = 1, 2, ..., K,$$

(K-1) is the number of conventional layers of the near-surface layer breakdown,

$\mu_0 = 4\pi \cdot 10^{-7}$ Hn/m is the magnetic constant,

μ_n is the absolute magnetic permeability of the region,

σ_n is the electrical conductivity of the region,

N is the total number of observation regions determined by the radii of the conventional layers,

$A(r_s, z_s)$ is the azimuthal component of the vector potential at the measurement point,

$I_0(\ ), I_1(\ )$ is modified Bessel functions of the first kind of zero and first orders of the complex argument,

$K_0(\ ), K_1(\ )$ is modified Bessel functions of the second kind of zero and first orders of the complex argument,

W is number of turns of the excitation coil,

r_{d1}, r_{d2} is inner and outer radii of the excitation coil, respectively,

l_{d1}, l_{d2} is distances to the excitation coil edges from the object,

r_s is radius of the measuring coil,

l_s is distance from the object to the measuring coil,

I is a sinusoidal excitation current with an angular frequency ω.

The dependence is significantly nonlinear and computationally expensive. Its use as a part of the objective function in optimization is unacceptable. Therefore, surrogate optimization involves replacing it with a metamodel [15] without these disadvantages.

4. Creating a neural network metamodel

The first stage of metamodel construction is the creation of a two-dimensional computer homogeneous experiment design (DOE) with low rates of discrepancies [16-18] based on LP_τ-Sobol's sequences, at the points of which the response is calculated according to the "exact" electrodynamic model. When constructing the DOE, it was taken into account that, in addition to the norm (sample) of the EC and MP profiles, there is their scatter within the technological tolerance δT, % both on the surface and at the depth of the TO.

For the two-dimensional DOE, a combination of LP_τ-sequences ξ_1, ξ_6 was used, which provides good indicators of centered CD and wrap-around WD, mixed MD, and weighted symmetrized centered WSCD discrepancy [19, 20], which together indicate the homogeneity of the created DOE. Subsequently, we scaled from a unit square to a rectangle of the real factor space, taking into account that the electrophysical parameters vary within the technological tolerance $\delta T = \pm 15$ %.

As a standard, i.e., a sample, obtained as a result of correct technological surface treatment of the TO, we took the profile of the EC, the minimum and maximum values for which are $\sigma_{min} = 3.494949 \cdot 10^6$ Sm/m, $\sigma_{max} = 6.99 \cdot 10^6$ Sm/m, and for the profile of the MP - $\mu_{r\,min} = 1$, $\mu_{r\,max} = 10$, respectively. Then the change in the parameters of the EC within the technological tolerance will be $2.971009 \cdot 10^6 \leq \sigma_{min} \leq 4.019162 \cdot 10^6$ Sm/m; and the MP - $8.5 \leq \mu_{r\,max} \leq 11.5$, with σ_{max} and $\mu_{r\,min}$ remaining unchanged. Other initial data required to determine the response at the DOE points are as follows: the radius of the TO $r = 10 \cdot 10^{-3}$ m, the excitation current frequency $f = 2.5 \cdot 10^3$ Hz, the thickness of the near-surface layer $D = 1 \cdot 10^{-3}$ m, which was subject to conditional division into $n = 51$ layers to obtain piecewise constant profiles of the distributions of electrophysical parameters.

Within the specified limits of changes in electrophysical parameters, the distribution of EC $\boldsymbol{\sigma}$ and MP $\boldsymbol{\mu_r}$ was calculated using a typical approximation - "hyperbolic tangent" [3] for the number of DOE points $N_{profile} = 5000$, which corresponds to the number of profiles in the total sample.

For the "technological" profiles of the MP and EC, which are established according to the created DOE, the EMF values were calculated using an electrodynamic model. As a result, we obtained a data array of size $N_{profile} \times (n_{\mu r} + n_\sigma)$, where $n_{\mu r}$, $n_\sigma = 51$ is the number of points of approximation of the MP and EC profiles (Table 1).

Table 1
Training sample size 5000×102 for creating metamodels

№ profile	$Re(e_{mod})$ 10^{-3}	$Im(e_{mod})$ 10^{-2}	σ_1 10^6, S/m	σ_2 10^6, S/m	...	σ_{51} 10^6, S/m	μ_{r1}	μ_{r2}	...	μ_{r51}
1	4.9468	4.2914	6.99	6.988266	...	3.237989	1	1.0036	...	8.7095
2	4.9815	4.5044	6.99	6.988148	...	2.980978	1	1.0042	...	10.4191
3	5.1623	4.3246	6.99	6.988513	...	3.772467	1	1.0038	...	9.1286
4	5.2418	4.5339	6.99	6.988395	...	3.515456	1	1.0045	...	10.8381
5	5.0194	4.3918	6.99	6.988276	...	3258446	1	1.0040	...	9.5476
...	...	...	...	...	...	...	...	...	...	...
4200	5.4592	4.5327	6.99	6.988621	...	4.004685	1	1.0046	...	10.9873
...	...	...	...	...	...	...	...	...	...	...

5000	5.3710	4.4928	6.99	6.988573		3.902054	1	1.0044		10.6039

The PCA method based on the SVD decomposition was applied to the obtained volume sample of 5000×102. As a result, 46 influential factors with eigenvalues greater than 1 were selected. To train deep MLP-neural networks (DNNs), we used a training set, which is a matrix of parameters in the latent factor space of size $N_{profile} \times n_{latent}$, where $n_{latent} = 46$ is the number of variables in this space. Of the total sample $N_{profile} = 5000$, 84 % of the profiles were selected for training neural networks, while the rest were not used in training, but some of them were later used as simulation profiles obtained by the ECP measurements to verify the reliability of the profile determination method.

The preliminary selection of the DNN architecture was carried out by the mean absolute error MAE (Mean Absolute Error), RMSE (Root Mean Square Error), and the coefficient of determination R2. This analysis showed the feasibility of using DNN with four hidden layers, a hyperbolic tangent activation function in each hidden layer, and the Levenberg-Marquardt learning method.

As a result, we obtained the Re-MLP-4-13-13-12-10-1 network for the real part of the EMF and the same Im-MLP-4-13-13-12-10-1 network for the imaginary part. The validity of the obtained metamodels was evaluated by the MAPE$_{metamod}$ errors, % (Mean Absolute Percentage Error) separately for the training, cross-validation, and test samples, the results of which are given in Table 2, and by analyzing the histograms of residuals (Fig. 1) and scatter plots.

Table 2
Mean Absolute Percentage Error MAPE$_{metamod}$, % of obtained metamodels

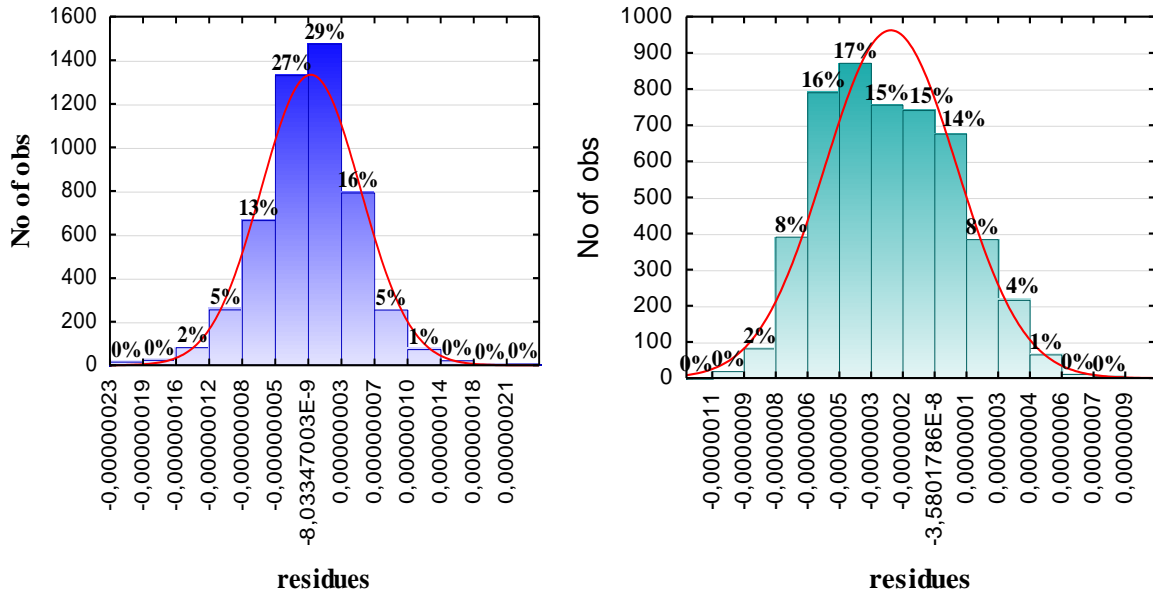| Metamodel	MAPE$_{metamod}$, %			
	Training sample, $N_{traine} = 3150$	Cross-validation sample, $N_{CV} = 525$	Test sample, $N_{test} = 525$	Across all profiles
Re-MLP-4-13-13-12-10-1	$7.644008 \cdot 10^{-4}$	$8.582822 \cdot 10^{-4}$	$8.402605 \cdot 10^{-4}$	$7.856487 \cdot 10^{-4}$
Im-MLP-4-13-13-12-10-1	$7.420608 \cdot 10^{-4}$	$7.525485 \cdot 10^{-4}$	$7.441971 \cdot 10^{-4}$	$7.436411 \cdot 10^{-4}$

Figure 1: Histograms of the residuals of the real and imaginary parts induced in the measuring turn of the ECP EMF for metamodels: a - Re-MLP-4-13-13-12-10-1; b - Im-MLP-4-13-13-12-10-1

The verification of the obtained metamodels was carried out by checking the correctness of the reproducibility of the response surface in the entire modeling area by the following statistical indicators: sums of squares of regression SS_D, residuals SS_R, total SS_T; middle squares of regression MS_D,

residuals MS_R, total MS_T; variances of reproducibility σ_D^2, adequacy σ_R^2, total σ_T^2; standard errors of reproducibility s_D, adequacy s_R, total s_T [21]. The numerical values of these indicators are given in Tables 3 and 4.

Table 3
Verification of the metamodel Re-MLP-4-13-13-12-10-1

Variance components ($N = 4200$)	Sum of squares	Middle square	Dispersion	Standard error
regressions	$SS_D = 8.563691 \cdot 10^{-5}$	$MS_D = 1.86167 \cdot 10^{-6}$ $v_D = 46$	$\sigma_D^2 = 2.03946 \cdot 10^{-8}$	$S_D = 1.4281 \cdot 10^{-4}$
residues	$SS_R = 1.241941 \cdot 10^{-11}$	$MS_R = 2.99047 \cdot 10^{-15}$ $v_R = 4153$	$\sigma_R^2 = 2.99047 \cdot 10^{-15}$	$S_R = 5.46852 \cdot 10^{-8}$
general	$SS_T = 8.564192 \cdot 10^{-4}$	$MS_T = 2.03958 \cdot 10^{-8}$ $v_T = 4199$	$\sigma_T^2 = 2.03958 \cdot 10^{-8}$	$S_T = 1.42814 \cdot 10^{-4}$

Table 4
Verification of the metamodel Im-MLP-4-13-13-12-10-1

Variance components ($N = 4200$)	Sum of squares	Middle square	Dispersion	Standard error
regressions	$SS_D = 4.395799 \cdot 10^{-3}$	$MS_D = 9.55609 \cdot 10^{-5}$ $v_D = 46$	$\sigma_D^2 = 1.04687 \cdot 10^{-6}$	$S_D = 1.02317 \cdot 10^{-3}$
residues	$SS_R = 6.459799 \cdot 10^{-10}$	$MS_R = 1.55545 \cdot 10^{-13}$ $v_R = 4153$	$\sigma_R^2 = 1.55545 \cdot 10^{-13}$	$S_R = 3.94392 \cdot 10^{-7}$
general	$SS_T = 4.397987 \cdot 10^{-3}$	$MS_T = 1.04739 \cdot 10^{-6}$ $v_T = 4199$	$\sigma_T^2 = 1.04739 \cdot 10^{-6}$	$S_T = 1.02342 \cdot 10^{-3}$

Verification of the adequacy and informativeness of the created metamodels was established according to the Fisher criterion [21] using the statistical indicators given in Tables 3, 4.

The value of Fisher's indicator for the obtained metamodel Re-MLP-4-13-13-12-10-1 is $F_{46;4153}^{total} = 6.225 \cdot 10^8$, and its critical value with a significance level of $\alpha = 5\%$ and the number of degrees of freedom $v_R = 4153$, $v_D = 46$, respectively $F_{0,05;46;4153}^{table} = 1.368$, which satisfies the adequacy condition. For the metamodel Im-MLP-4-13-13-12-10-1, the condition of adequacy according to this criterion is also met, since $F_{46;4153}^{total} = 6.144 \cdot 10^8$. The model was tested for informativeness by calculating the coefficient of determination R^2 and testing the hypothesis of the significance of this coefficient by Fisher's criterion. The coefficient of determination for both metamodels exceeds 0.999, which indicates their high informativeness. These coefficients are significant at the 5 % significance level, since the condition of informativeness is met for both metamodels ($F_{46;4153}^{total} = 1.8144 \cdot 10^5$).

5. Numerical experiments and their discussion

Numerical experiments consisted in solving the inverse measurement problem by an optimization hybrid population metaheuristic method based on simulating three measurements of the EMF signal using ECPs, i.e., their amplitude and phase, and the surrogate model created in the previous step.

To efficiently create a target function for finding the optimal values of the desired model parameters, the measured signal is represented in the algebraic form $e_{mes} = C_{mes} + j \cdot D_{mes}$, where C_{mes} and D_{mes} are its real and imaginary parts, respectively.

A series of starts of the optimization algorithm was performed and forty-eight reconstructions of the modified MP and EC profiles were obtained for three measurements. Table 5 shows the obtained values of MAPE errors for all individual solutions of μ_r and σ.

Table 5
Relative error values for the reconstructed profiles of MP and EC based on the results of averaging

№ start of the optimization algorithm	MAPE, %					
	e_{mes1}		e_{mes2}		e_{mes3}	
	$C_{mes} = 0.00546261$ $D_{mes} = 0.0459517$		$C_{mes} = 0.00534846$ $D_{mes} = 0.0442374$		$C_{mes} = 0.0053832$ $D_{mes} = 0.0451805$	
	μ_r	σ	μ_r	σ	μ_r	σ
1	0.417	0.403	2.031	0.634	1.342	1.535
2	0.358	0.671	2.865	1.958	0.531	0.711
3	0.372	0.673	0.826	0.667	0.775	1.138
4	0.241	0.529	0.279	0.728	1.070	1.492
5	0.279	0.318	0.269	0.743	3.239	1.202
6	0.055	0.182	0.205	0.349	0.209	1.203
7	0.501	0.765	0.415	0.279	0.434	1.789
8	0.015	0.234	0.114	0.413	1.399	0.989
9	0.294	0.43	0.290	0.150	0.674	0.334
10	0.322	0.561	0.375	0.773	0.745	0.056
11	0.402	0.684	0.960	0.918	0.504	1.379
12	0.379	0.405	0.962	0.826	0.248	1.690
13	0.104	0.082	0.543	0.145	3.281	2.568
14	0.151	0.103	0.833	1.652	0.761	0.712
…	…	…	…	…	…	…
46	0.239	0.396	0.585	0.465	1.08	1.286
47	0.032	0.109	1.802	1.079	0.748	0.321
48	0.753	0.581	1.288	0.872	3.65	1.862

The values of the technological profiles of the MP $\mu_{r\,tech}$ and reconstructed $\mu_{r\,recon}$, obtained by averaging the calculation data for all three measurements, and the values of the relative errors at each point of the profiles δ_i, % are given in Table 6. The same, but for the EC profiles, is given in Table 7. The obtained values of the errors MAPE, % for each of the three measurements separately for the MP and EC profiles are shown in Fig. 2.

Table 6
Values of the technological and reconstructed profiles of the MP

№ of conventional layer	e_{mes1}			e_{mes2}			e_{mes3}		
	$C_{mes} = 0.00546261$ $D_{mes} = 0.0459517$			$C_{mes} = 0.00534846$ $D_{mes} = 0.0442374$			$C_{mes} = 0.0053832$ $D_{mes} = 0.0451805$		
	Profile $\mu_{r\,tech}$	Profile $\mu_{r\,recon}$	Relative error, δ_i, %	Profile $\mu_{r\,tech}$	Profile $\mu_{r\,recon}$	Relative error, δ_i, %	Profile $\mu_{r\,tech}$	Profile $\mu_{r\,recon}$	Relative error, δ_i, %
1	1	1.0036	0.3630	1	1.0032	0.3193	1	0.9966	0.3373
2	1.0049	1.0085	0.3592	1.0042	1.0074	0.3196	1.0046	1.0011	0.3380
3	1.0067	1.0103	0.3577	1.0058	1.0090	0.3197	1.0062	1.0028	0.3383
4	1.0092	1.0128	0.3557	1.0080	1.0111	0.3200	1.0086	1.0052	0.3387
5	1.0127	1.0162	0.3531	1.0109	1.0141	0.3202	1.0118	1.0084	0.3393
…	…	…	…	…	…	…	…	…	…
47	11.4827	11.4410	0.3627	10.0347	10.0742	0.3929	10.8058	10.7527	0.4917
48	11.4861	11.4445	0.3627	10.0377	10.0771	0.3929	10.8091	10.7559	0.4917
49	11.4887	11.4470	0.3627	10.0399	10.0793	0.3929	10.8114	10.7583	0.4917
50	11.4905	11.4488	0.3627	10.0415	10.0809	0.3929	10.8131	10.7600	0.4917
51	11.4918	11.4501	0.3627	10.0426	10.0821	0.3929	10.8144	10.7612	0.4917

Table 7
Values of technological and reconstructed profiles of the EC

№ of conventional layer	e_{mes1} $C_{mes}=0.00546261$ $D_{mes}=0.0459517$			e_{mes2} $C_{mes}=0.00534846$ $D_{mes}=0.0442374$			e_{mes3} $C_{mes}=0.0053832$ $D_{mes}=0.0451805$		
	Profile σ_{tech} 10^6, Sm/m	Profile σ_{recon} 10^6, Sm/m	Relative error, δ_i, %	Profile σ_{tech} 10^6, Sm/m	Profile σ_{recon} 10^6, Sm/m	Relative error, δ_i, %	Profile σ_{tech} 10^6, Sm/m	Profile σ_{recon} 10^6, Sm/m	Relative error, δ_i, %
1	6.99	7.01537	0.3630	6.99	7.01232	0.3193	6.99	6.96642	0.3373
2	6.98855	7.01392	0.3630	6.98863	7.01094	0.3192	6.98856	6.96499	0.3373
3	6.98801	7.01337	0.3630	6.98811	7.01042	0.3192	6.98801	6.96445	0.3373
4	6.98726	7.01262	0.3630	6.98740	7.00970	0.3192	6.98727	6.96370	0.3373
5	6.98623	7.01158	0.3630	6.98642	7.00872	0.3192	6.98624	6.96267	0.3373
…	…	…	…	…	…	…	…	…	…
47	3.86161	3.87379	0.3155	4.02175	4.03096	0.2291	3.87166	3.85753	0.3649
48	3.86058	3.87276	0.3154	4.02077	4.02998	0.2290	3.87063	3.85650	0.3649
49	3.85983	3.87200	0.3154	4.02006	4.02926	0.2290	3.86988	3.85576	0.3650
50	3.85928	3.87146	0.3154	4.01954	4.02874	0.2290	3.86934	3.85522	0.3650
51	3.85889	3.87106	0.3154	4.01916	4.02836	0.2290	3.86894	3.85482	0.3650
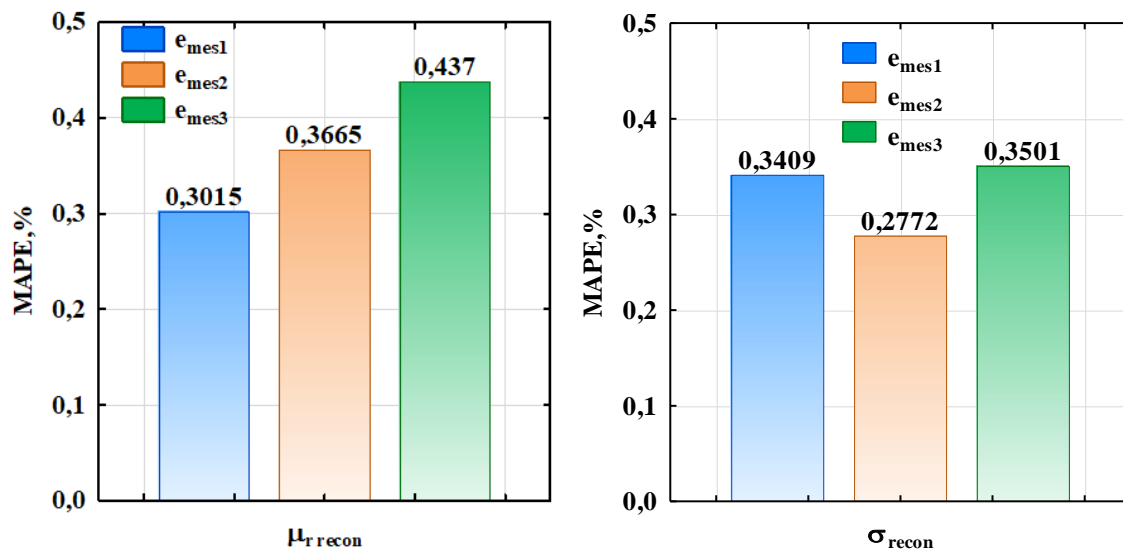
Figure 2: MAPE errors, % for each of the three measurements separately for the MP and EC profiles

6. Acknowledgements

created on deep fully connected neural networks, the approximation errors of the $MAPE_{metamodel}$ of which do not exceed $7.4364 \cdot 10^{-4}$ % and $7.8565 \cdot 10^{-4}$ %, respectively, for the real and imaginary parts of the EMF. The adequacy and informativeness of the constructed metamodels have been proved. According to Fisher's criterion, both metamodels are adequate with a significance level of 5 %, where the criterion indicator is not worse than, and informative with a determination coefficient of more than 0.999. Numerical modeling experiments have demonstrated the reliability of profile reconstruction with acceptable accuracy. Thus, we obtained MAPE error values that do not exceed 0.437 % and 0.36 %, respectively, for the MP and EC profiles.

7. References

[1] N. Bowler, Eddy-current nondestructive evaluation, Springer, New York, 2019.

[2] N. Ida, N. Meyendorf, eds, Handbook of advanced nondestructive evaluation, volume 10, Cham. Switzerland: Springer International Publishing, 2019.

[3] V. Y. Halchenko, V. V. Tychkov, A. V. Storchak, R. V. Trembovetska, Reconstruction of surface radial profiles of electrophysical characteristics of cylindrical objects during eddy current measurements with a priori data. The selection formation for the surrogate model construction, Ukrainian Metrological Journal 1 (2020), 35-50. doi:10.24027/2306-7039.1.2020.204226.

[4] R. Trembovetska, V. Halchenko, C. Bazilo, Inverse multi-parameter identification of plane objects electrophysical parameters profiles by eddy-current method, Smart Technologies in Urban Engineering: Proceedings of STUE-2022, Cham: Springer International Publishing, 2022, 202-212. doi:10.1007/978-3-031-20141-7_19.

[5] H. Tesfalem, J. Hampton, A. D. Fletcher, M. Brown, A. J. Peyton, Electrical resistivity reconstruction of graphite moderator bricks from multi-frequency measurements and artificial neural networks, IEEE Sensors Journal 21(15) (2021), 17005-17016. doi:10.1109/JSEN.2021.3080127.

[6] H. Tesfalem, A. J. Peyton, A. D. Fletcher, M. Brown, B. Chapman, Conductivity profiling of graphite moderator bricks from multifrequency eddy current measurements, IEEE Sensors Journal 20(9) (2020) 4840-4849. doi:10.1109/JSEN.2020.2965201.

[7] J. Xu, J. Wu, W. Xin, Z. Ge, Measuring ultrathin metallic coating properties using swept-frequency eddy-current technique, IEEE Transactions on Instrumentation and Measurement 69(8) (2020) 5772-5781. doi:10.1109/TIM.2020.2966359.

[8] P. Huang, J. Zhao, Z. Li, H. Pu, Y. Ding, L. Xu, Y. Xie, Decoupling Conductivity and Permeability Using Sweep-Frequency Eddy Current Method, IEEE Transactions on Instrumentation and Measurement 72 (2023) 1-11. doi:10.1109/TIM.2023.3242017.

[9] V. Y. Halchenko, A. V. Storchak, R. V. Trembovetska, V. V. Tychkov, The creation of a surrogate model for restoring surface profiles of the electrophysical characteristics of cylindrical objects, Ukrainian Metrological Journal 3 (2020) 27-35. doi:10.24027/2306-7039.3.2020.216824.

[10] V. Halchenko, A. Storchak, V. Tychkov, R. Trembovetska, Measurements of near-surface radial profiles of electrophysical characteristics of cylindrical objects by the eddy current method using a priori data, Ukrainian Metrological Journal 1 (2022) 5–11. doi:10.24027/2306-7039.1.2022.258678.

[11] R. Boiger, R. L. Modini, A. Moallemi, D. Degen, A. Adelmann, M. Gysel-Beer, Retrieval of aerosol properties from in situ, multi-angle light scattering measurements using invertible neural networks, J. Aerosol Sci, volume 163 (2022) 105977. doi:10.1016/j.jaerosci.2022.105977.

[12] P. Jiang, Q. Zhou, X. Shao, Surrogate-Model-Based Design and Optimization, In: Surrogate Model-Based Engineering Design and Optimization, Springer Tracts in Mechanical Engineering, Springer, Singapore, 2020. doi:10.1007/978-981-15-0731-1_7 1.

[13] S. Ullah, D. A. Nguyen, H. Wang, S. Menzel, B. Sendhoff, T. Bäck, Exploring Dimensionality Reduction Techniques for Efficient Surrogate-Assisted optimization, In 2020 IEEE Symposium Series on Computational Intelligence, SSCI 2020, Canberra, Australia, December 1-4, 2020, IEEE, 2965–2974. doi:10.1109/SSCI47803.2020.9308465.

[14] C. V. Dodd, J. W. Luquire, W. E. Deeds, W. G. Spoeri, Some eddy-current problems and their integral solutions, United States: NSA-23-024407, 1969 89. doi:10.2172/4783007.

[15] B. Kuznetsov, I. Bovdui, T. Nikitina, V. Kolomiets, B. Kobylianskyi, Surrogate synthesis of system of active shielding of magnetic field generated by group of overhead power lines, EUROCON 2021 - 19th IEEE International Conference on Smart Technologies, Proceedings, 2021 381–384. doi:10.1109/EUROCON52738.2021.9535630.

[16] K. Fang, M. Q. Liu, H. Qin, Y. D. Zhou, Theory and application of uniform experimental designs, Singapore: Springer, 2018.

[17] H. Ping, D. K. Lin, L. Min-Qian, X. Qingsong, Z. Yongdao, Theory and application of uniform designs, SCIENTIA SINICA Mathematica 50 (2020) 561. doi:10.1360/SSM-2020-0065.

[18] Y. Wang, F. Sun, H. Xu, On design orthogonality, maximin distance, and projection uniformity for computer experiments, Journal of the American Statistical Association 117(537) (2022) 375-385. doi:10.1080/01621459.2020.1782221.

[19] X. Ke, R. Zhang, H. J. Ye, Two-and three-level lower bounds for mixture L2-discrepancy and construction of uniform designs by threshold accepting, Journal of Complexity, 31(5) (2015) 741-753. doi:10.1016/j.jco.2015.01.002.

[20] L. He, H. Qin, J. Ning, Weighted symmetrized centered discrepancy for uniform design, Communications in Statistics-Simulation and Computation, 51(8) (2020) 1-11. doi:10.1080/03610918.2020.1744063.

[21] C. M. Douglas, Design and analysis of experiments, Wiley, London, 2009.